RSC Advances

PAPER

View Article Online
View Journal | View Issue

Cite this: *RSC Adv.*, 2025, **15**, 11934

Tailoring ultra-small ZnO nanoparticles through cobalt doping to enhance photocatalytic CO_2 reduction†

Wen-zhu Yang,‡[a] Imran Ullah,‡*[b] Zhan-Guo Jiang,[a] Reinhard B. Neder*[b] and Cai-Hong Zhan*[a]

Received 26th February 2025
Accepted 9th April 2025

DOI: 10.1039/d5ra01374g

rsc.li/rsc-advances

Photocatalytic CO_2 reduction offers a promising pathway for achieving sustainable development. However, the effectiveness of this method faces challenges related to imbalanced charge transfer/utilization. To address these issues, this paper reports on cobalt-doped zinc oxide nanoparticles (Co-ZnO NPs). The cobalt doping not only increases light absorption but also improves charge transfer/separation kinetics and modulates the reduction reaction dynamics. Notably, photocatalytic tests show that cobalt-doped zinc oxide (Co-ZnO) achieves a CO yield of 143.90 μmol g^{-1} h^{-1}, which is 15.73 times higher than that of undoped ZnO, and exhibits excellent stability. This study emphasizes the importance of polarization states induced by doping for achieving efficient charge separation, providing a new approach to enhance the efficiency of photoredox catalysis.

Introduction

Climate change's vast and multifaceted impact on the earth's delicate ecosystems and human societies, especially in developing countries, has become irrefutable in recent years.[1–3] Since the mid-1800s, the temperatures of the land and ocean have climbed by an average of 0.06 °C per decade[4,5] with an even sharper rise (0.2 °C) observed since the 1980s.[4–6] An increase of 1.5 °C by 2050 and 2 °C to 4 °C by 2100 is estimated due to the accumulation of greenhouse gases,[9] primarily carbon dioxide (CO_2), methane (CH_4), nitrous oxide (N_2O), and fluorinated gases.[7–14] It is linked to burning fossil fuels and deforestation. Recent studies reveal that CO_2 makes up a staggering 76% of human-generated greenhouse gases and is a major contributor to climate change.[15–18] Unfortunately, the long atmospheric lifetime and stable molecular structure of CO_2 make it less reactive with a high standard Gibbs free energy of −394.39 kJ mol^{-1}.[19–22] Capturing and utilizing existing CO_2 is essential. Several strategies have emerged to address the challenge, including photocatalysis, electrochemical approaches, thermal catalysis, biological approaches, and chemical reduction.[23–27] Methane (CH_4) or other hydrocarbons can be produced by reacting CO_2 with hydrogen gas (H_2) in the presence of a suitable catalyst (hydrogenation), whilst in biocatalysis, specific enzymes act as catalysts to promote CO_2 reduction.[28,29] Every approach has some pros and cons.

Photocatalysis offers a sustainable, non-toxic, and environmentally friendly approach, utilizing light energy to convert CO_2 into value-added products,[32,33] such as carbon monoxide (CO), CH_4, methanol, or other hydrocarbons.[30–32] Extensive research has been pursued to design efficient photocatalysts with unique capabilities.[33–36] Materials with sizes ranging from a few nanometres (nm) to 100 nm having a high surface-to-volume ratio and size-dependent properties due to the quantum confinement effect are classified as nanomaterials.[37–39] Their properties are much different than bulk, making them specific attention to various fields, namely electronics, energy storage, medicine, the food industry, catalysis, and agriculture.[40–45] However, despite their promise, several challenges remain, including low quantum yield, bandgap limitation, surface poisoning, mass transport limitations, and ensuring long-term stability.[46] In the early 1970s, Akira Fujishima and Kenichi Honda demonstrated the potential of titanium dioxide (TiO_2) NPs as photocatalysts, capable of splitting water using ultraviolet (UV) light radiation.[47] This discovery sparked a surge in research, leading to the exploration of various semiconductor nanomaterials (ZnO, CdS, MoS_2) for their photocatalytic activities in the late 1990s.[47–51] Researcher use new methods to synthesize nanomaterials with varied shapes, compositions, and surface properties. The sol–gel route is notable for producing nanoparticles under 10 nm with diverse shapes and morphologies.[52–55] Such magic-size particles are explored employing complementary characterization techniques, such as X-ray diffraction (XRD), ultraviolet-

[a]*Key Laboratory of the Ministry of Education for Advanced Catalysis Material, College of Chemistry and Materials Science, Zhejiang Normal University, Jinhua 321004, China. E-mail: imran.ullah@fau.de; chzhan@zjnu.cn*

[b]*Institute for Crystallography and Structural Physics, Friedrich-Alexander University Erlangen-Nurnberg, Staudtstr. 3, Erlangen 91058, Germany. E-mail: reinhard.neder@fau.de*

† Electronic supplementary information (ESI) available. See DOI: https://doi.org/10.1039/d5ra01374g

‡ These authors contributed equally to this work.

visible (UV-vis) spectroscopy, infra-red Fourier transform (FT-IR) spectroscopy and further details can be found in ref. 56. The use of photocatalysts extends beyond CO_2 reduction and employed for various environmental and energy applications since the early 2000s. These applications include water purification, air pollution remediation, and hydrogen production.[57–60] Furthermore, pioneering research by Ola *et al.* explored TiO_2 NPs as promising photocatalysts for CO_2 reduction.[61] The CO_2 reduction involves two key steps, adsorption of CO_2 on the active sites of NPs surface (adsorb either as individual CO_2 molecules or as surface carbonates) and photo-induced redox reaction (oxidation and reduction).[62,63] These two steps can be improved by tailoring the surface properties and band gap engineering through incorporating transition metals. Adding ligand molecules with functional groups like carboxylates or hydroxyls improves CO_2 adsorption by forming strong chemical bonds. These ligands also create smoother pathways for charge carriers, speeding up reactions and reducing electron–hole recombination.[64] The formation of faceted NPs is characteristic of ligand-capping and hence enhances the durability of NPs.[64,65] Moreover, transition metal incorporation alters surface properties resulting in the formation of new active sites and promoting the direct sticking of CO_2 molecules.[66–69]

As the prominent features include simple composition, low cost, high stability, easy synthesis, and nontoxicity, this study focuses on the synthesis of ZnO NPs with tailored properties for CO_2 reduction. We employed the sol–gel route to achieve the desired size and shape control of the NPs. Two different aspects of our study are to improve the CO_2 adsorption capabilities and promoting efficient charge separation of photocatalysts by introducing ligand molecules as capping agents and transition metal as doping agents. Further, the bandgap is tailored by incorporating transition metal, cobalt (Co). This modification can potentially enhance light absorption by a photocatalyst, leading to improved CO_2 conversion efficiency. The preliminary confirmation of the structure of the metal incorporation was revealed from XRD data of the synthesized photocatalysts. No secondary phase segregation was seen. Optical and electronic properties were investigated using UV-vis spectroscopy. The elemental composition, chemical states, and surface chemistry of the NPs were explored using XPS studies. The transient photocurrent response under visible-light irradiation was measured and indicates that cobalt doped ZnO NPs have a stronger photogenerated carrier lifetime and outstanding separation ability. The work here represents an important case study for the development of photosensitive and higher photogenerated charge transfer efficiency ZnOs for artificial photoreduction of CO_2.

Result and discussion

The sol–gel method (bottom-up approach) introduced by Spanhel and Anderson with several modifications by Wood *et al.*, Chory *et al.*, and Ullah *et al.* was used to obtain NPs of the desired size in the present work.[70–73] The procedure involves three steps: metal salt's dissolution in organic solvent (ethanol, methanol *etc.*), the addition of base, and the addition of precipitator. The synthesis starts by dissolving 0.61043 g zinc acetate dihydrate ($(CH_3COO)_2{\cdot}Zn{\cdot}2H_2O$) in 100 mL absolute ethanol (27 mM) at room temperature through magnetic stirring at the speed of 300 revolutions per minute (rpm). An optimized amount (0.52 mM) of ligand molecules (for capped NPs) is added at the first stage with zinc precursor. The solution is stirred till it becomes transparent. The adsorption of ligand molecules on certain crystal faces disrupts or slows down the growth kinetics. An organic base, tetra-methyl ammonium hydroxide (25% in methanol) (TMAH), of 3 mL is added gradually to achieve the desired pH (9–12). Upon base addition, the solution becomes cloudy in most cases, while for dmlt (dimethyl-L-tartrate) it takes 6–9 hours. Gel formation can be observed directly as confirmation of the NPs growth. Precipitator, a mixture of 12 mL Hexane and 8 mL acetone, is used to promote the gel formation further. The gel is centrifuged at the speed of 4000 rpm and washed with acetone three times. Every time the supernatant is discarded. The sediment is put in a desiccator overnight to dry at room temperature without additional treatment.

For the synthesis of cobalt-doped zinc oxide nanoparticles (Co-ZnO NPs), an optimized amount of corresponding precursor (cobalt acetate tetrahydrate($(CH_3COO)_2{\cdot}Co{\cdot}4H_2O$)) was added alongside zinc acetate dihydrate at the beginning of the process. Chemicals (analytical grade, Sigma-Aldrich and Roth) were used without further purification. Glassware was cleaned with DI water, followed by immersion in 1% HCl (hydrochloric acid) and 1% NaOH (sodium hydroxide) solution, and finally rinsed thoroughly with DI water and dried at 110 °C.

Among fascinating semiconductors, ZnO crystallizes in a hexagonal Wurtzite crystal structure, where each zinc ion (Zn^{2+}) is surrounded by four oxygen ions (O^{2-}). The combination forms tetrahedral coordination and results in ZnO_4 corner-sharing tetrahedra with three shorter and one longer Zn–O bond length. Conversely, the O^{2-} ion is bound to four Zn^{2+} ions. ZnO belonging to a space group $P6_3mc$ (No. 186) with lattice parameters, $a = b = 3.24920$ and $c = 5.2700$ Å and $\alpha = \beta = 90^{\circ}$ and $\gamma = 120^{\circ}$. The c/a ratio for ideal structure is ≈ 1.66. The structure is shown in Fig. 1b.

Fig. 1c illustrates the powder X-ray diffraction (PXRD) of all synthesized samples. The diffraction peaks correspond to specific crystallographic planes within the material, (100), (002), (101), (102), (110), (103) and (112), consistent with the hexagonal space group $P6_3mc$ (No. 186). These results are in excellent agreement with the card entry JCPDS No. 36-1451. The presence of well-defined peaks indicates crystalline nature of all synthesized samples, and their broadness (full width at half maximum, FWHM) suggests the formation of ultra-small NPs. The broader FWHM of the (102) reflection is not unusual and is commonly observed in Wurtzite-type materials, typically attributed to the presence of stacking faults.

The contents of elements in Co-doped ZnO NPs were analyzed from the EDS images of the samples (Fig. 1e and S5†), it can be seen that there are characteristic peaks of Zn, Co, O, and C elements in ZnO-5%Co-cit and ZnO-5%Co-dmlt. The cobalt element content corresponds to the percentage content, which once again proves that cobalt doped ZnO NPs have been

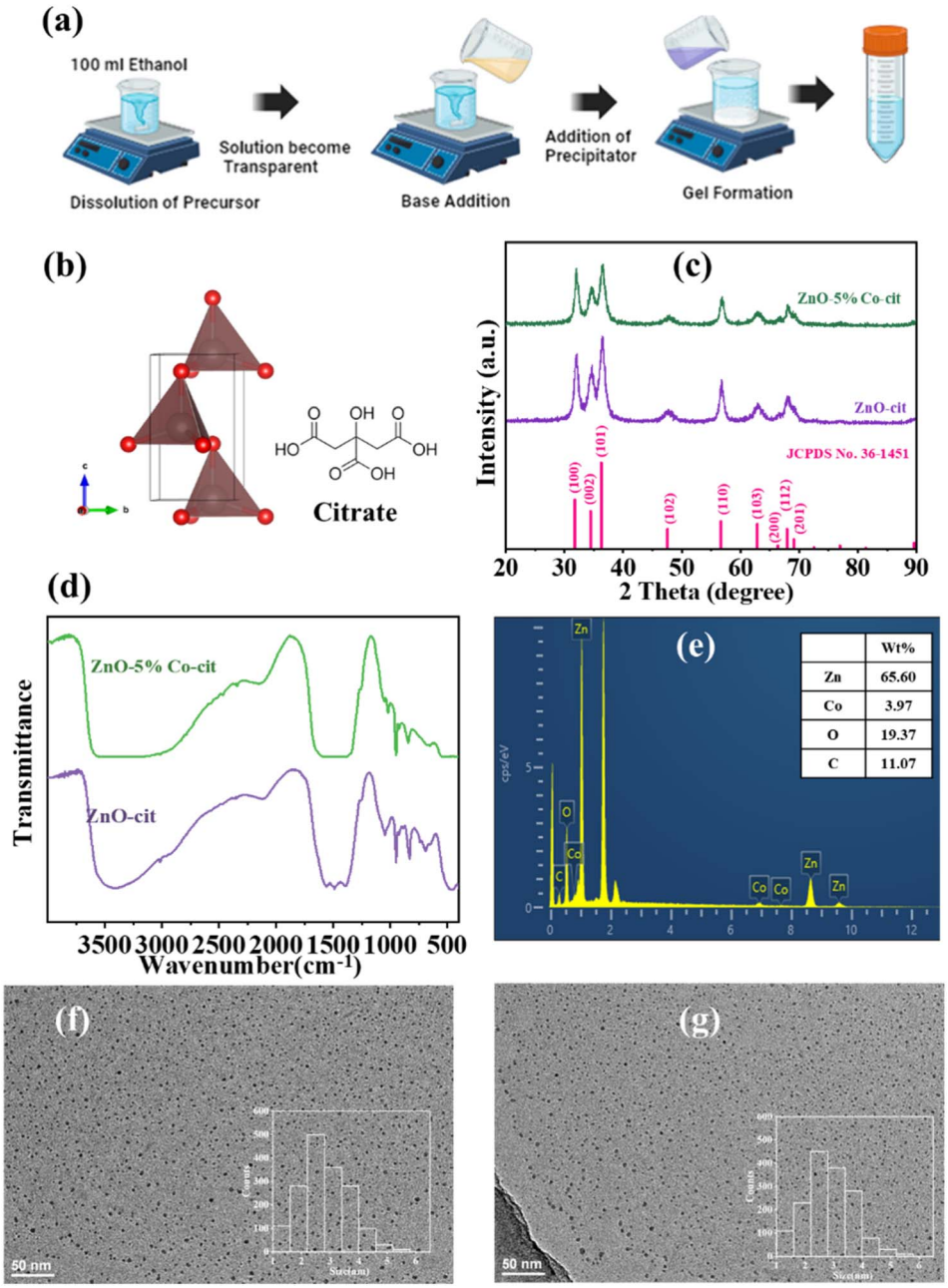

Fig. 1 Synthesis and spectroscopic characterizations: (a) schematic illustrating the synthetic procedure of ZnO and ZnO-5%Co-cit; (b) crystal Structure of ZnO; (c) XRD patterns (d) IR spectra of ZnO and ZnO-5%Co-cit; (e) EDS mapping images of ZnO-5%Co-cit; TEM images of (f) ZnO-cit and (g) ZnO-5%Co-cit.

successfully prepared. Fig. 1f and g show the TEM images of the synthesized ZnO and Co-ZnO NPs with sizes of approximately 3 nm.

Transition metal dopants introduce electron-deficient sites on the catalyst surface. These sites polarize CO_2 molecules through strong Lewis acid–base interactions, facilitating CO_2 chemisorption. Dopant-induced oxygen vacancies serve as preferential adsorption centers, lowering the energy barrier for CO_2 activation. The stabilization of key intermediates is further enhanced *via* M–O–C bonding motifs. The spatial separation of photogenerated carriers near dopant sites creates localized electric fields, which synergistically strengthen CO_2 adsorption through dipole interactions.[74]

The photocatalytic CO_2 reduction activity of different samples was tested under visible light irradiation, as shown in Fig. 2a. The cobalt doped ZnO NPs exhibited excellent CO_2 reduction activity. The yield of C_1-compound in ZnO-5%Co-cit reached 143.90 μmol g^{-1} h^{-1} (much higher than other ZnO complexes reported, see Table S2†), which is 15.73 times higher than that of undoped ZnO-cit. During this process, a large amount of CO was generated, and for ZnO-5%Co-cit, the selectivity of CO_2 to CO conversion reached 53.5%. In addition,

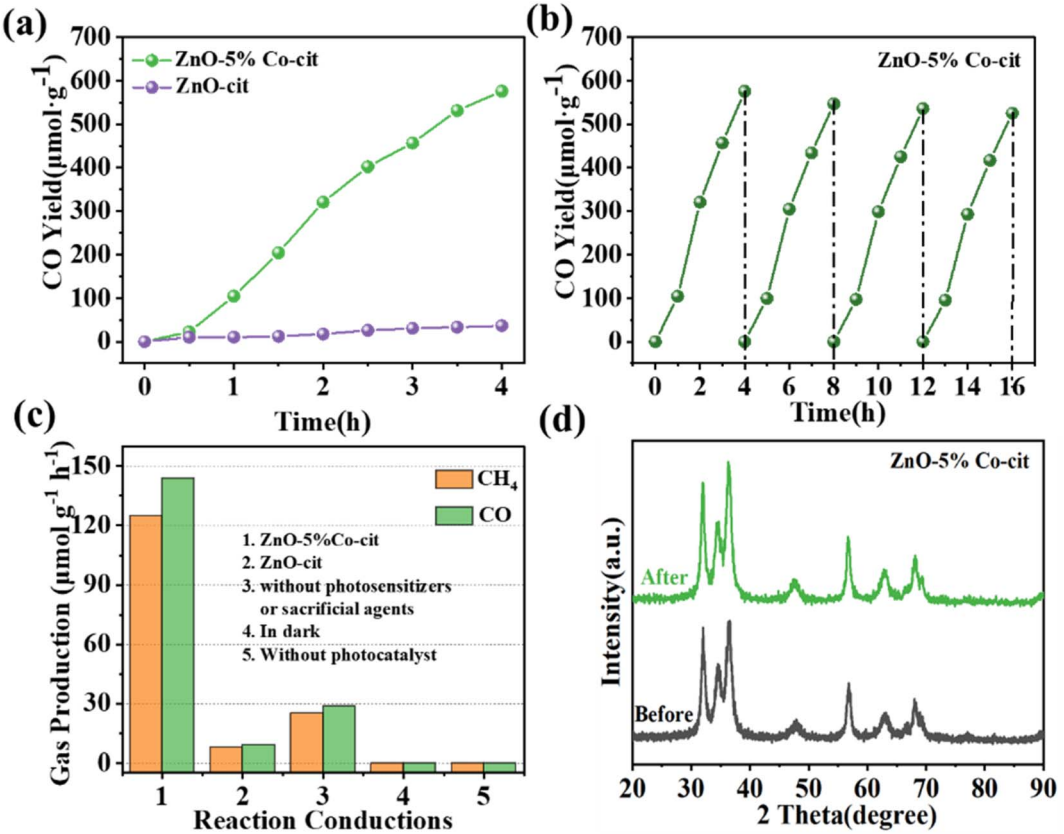

Fig. 2 Photocatalytic performance: (a) photocatalytic CO evolution (light source:300 W Xe lamp, $\lambda > 420$ nm), (b) Cycling test of ZnO-5%Co-cit for the photocatalytic CO evolution, (c) CH_4 and CO evolution rates under different reaction conductions, (d) XRD patterns of ZnO-5%Co-cit before and after photocatalytic tests.

cyclic testing was conducted on ZnO-5%Co-cit, and its photocatalytic CO_2 reduction performance remained almost unchanged after four cycles (4 hours per cycle) (Fig. 2b), and there was no significant change in XRD before and after the reaction (Fig. 2d), indicating that ZnO-5%Co-cit has good stability.

The photogenerated carrier dynamics of ZnO and Co-ZnO NPs were comparatively investigated by a series of techniques. (The electronic band structures of the two NPs were investigated using UV-vis DRS and Mott–Schottky measurements.) As shown in Fig. 3a, the UV-vis absorption spectra show that ZnO-5%Co-cit exhibit higher light absorption capacity than ZnO-cit in the range of >400 nm. The bandgap width of semiconductor materials can be calculated based on the Tauc formula $(\alpha h\nu)^{1/n} = A(h\nu - E_g)$. In this photocatalytic system, ZnO is a direct bandgap semiconductor, so we take $n = 1/2$ and plot the $(\alpha h\nu)^2$–hν variation relationship curve. The results are shown in Fig. 3b, the optical band gaps of ZnO-5%Co-cit to be 2.45 eV.[75] The steady-state photoluminescence (PL) spectroscopy reveals that the quenching intensity of the Co-ZnO NPs are significantly lower than that the undoped ZnO NPs (Fig. 3d), manifesting cobalt doping can improve the separation efficiency of electrons and holes. Further investigation of the band structure of ZnO NPs was conducted through the Mott–Schottky test. The positive slope curves can be seen in Fig. 3c, indicating the n-type semiconductor for ZnO NPs. The Mott–Schottky plots were obtained for three different frequencies (800 Hz, 1500 Hz, and 2000 Hz) to verify the CB of ZnO-5%Co-cit, resulting in values of −0.72 V *vs.* NHE. The EIS Nyquist plots of the samples reveal the relationship between carrier transport and charge transfer impedance on the catalyst surface. From the Fig. 3e, it can be seen that the order of EIS Nyquist arc radius is: ZnO-cit > ZnO-5%Co-cit. Among them, the sample of ZnO-5%Co-cit has better conductivity, faster photo generated carrier transport efficiency, and better charge separation ability. From the transient photocurrent response diagram of the samples (Fig. 3f), it can be seen that compared to undoped ZnO NPs, the cobalt doped ZnO NPs exhibits stronger photocurrent response, indicating that Co-ZnO NPs have stronger photogenerated carrier lifetime and outstanding separation ability. It can efficiently transfer it to the electrode and effectively suppress the recombination behavior of photogenerated carriers, resulting in the best photocatalytic activity. This is consistent with the analysis results of photoluminescence spectra and impedance spectra. The above discussions collectively prove that cobalt doped ZnO NPs contribute to the separation and transportation of photogenerated carriers, suppress the recombination of electrons and holes, extend electron lifetime, and further optimize the photocatalytic performance of the materials.

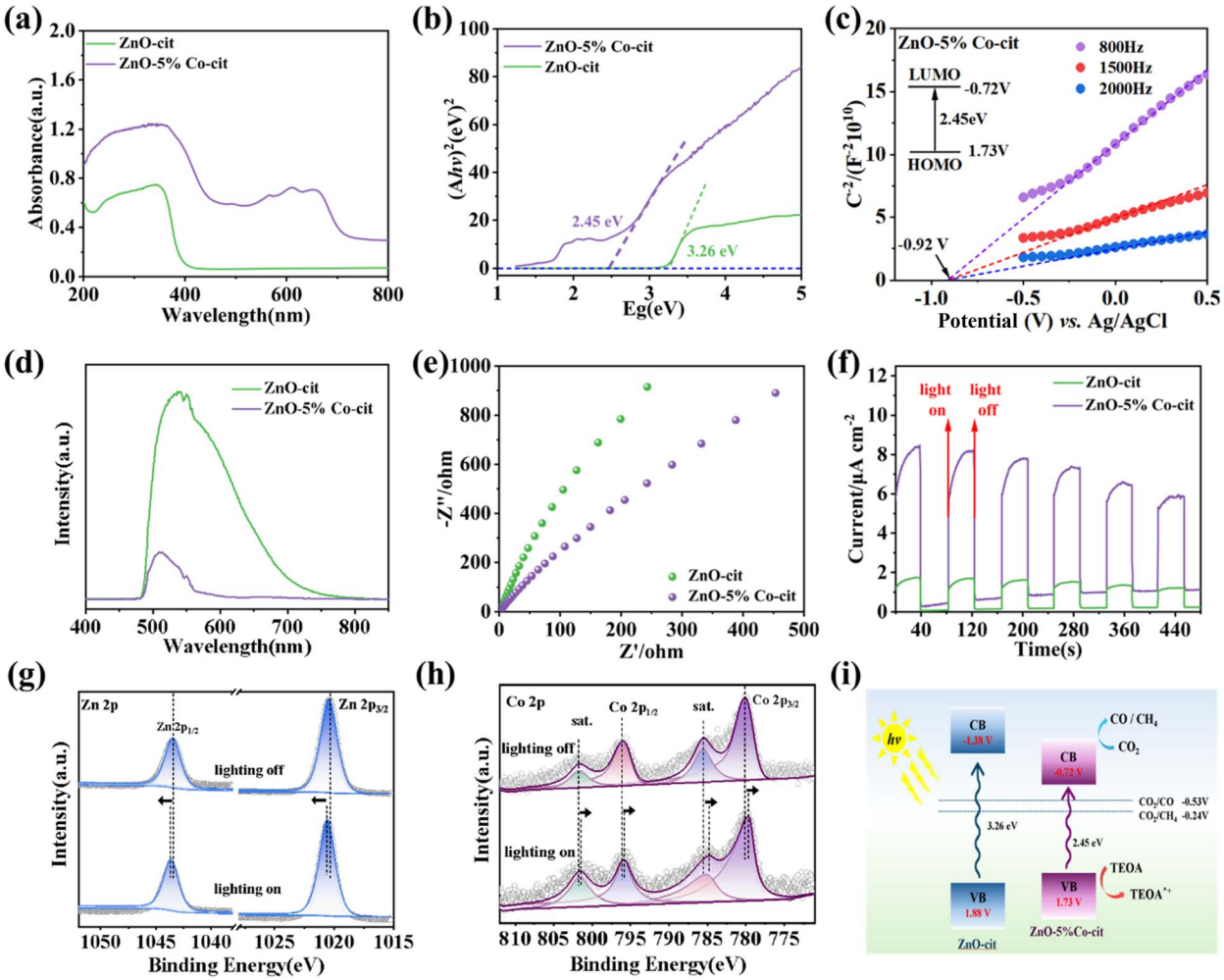

Fig. 3 Charge transfer mechanism analysis: (a) UV-vis diffuse reflectance spectra (b) Tauc plots (c) Mott–Schottky plots and energy band structures; (d) PL spectra; (e) Nyquist plots; (f) photocurrent responses of ZnO-cit and ZnO-5%Co-cit; *in situ* irradiated XPS spectra of ZnO-5% Co-cit: (g) Zn 2p (h) Co 2p; (i) schematic illustrating the charge transfer mechanisms in ZnO and ZnO-5%Co-cit.

In order to determine the charge transfer pathway of the doped samples, we conducted *in situ* XPS testing, as shown in Fig. 3g and h. Compared with ZnO-5%Co-cit in the dark, the binding energy of Zn 2p in the doped sample significantly shifted to a higher binding energy level under illumination, while Co 2p shifted towards a lower binding energy level, indicating that under illumination, the photogenerated electrons in ZnO NPs transfer to the doped cobalt ions. Enhancing interface electron transfer through high-speed electronic transmission channels can ensure timely consumption of photogenerated holes in ZnO NPs, alleviate the process of photo corrosion, and improve the stability of the photocatalytic system. And the hole sacrificial agent TEOA (triethanolamine) was added in the reaction system. Meanwhile, the consumption of more photogenerated holes will lead to the production of more photogenerated electrons, promoting the conversion of CO_2 to CO and CH_4.

The spin polarized (SP) band structures and density of states of pristine ZnO and Co-doped ZnO system were calculated to probe the effect of Co substitution and the origins of the electrical properties. As shown in Fig. S2,† compared with the pristine ZnO, the significant feature of Co-doped ZnO is that the impurity state (IS) appears between the conduction bands (CBs) and valence bands (VBs). To further study the modifications in the band structure of doped system, the total and partial density of states are computed. Fig. S2† illustrates the total and partial DOSs of Co-doped ZnO. It is notable that the impurity state is derived from the Co-d state, which further attests the photogenerated electrons in ZnO NPs will transfer to the doped cobalt ions. We can also see that spin channels have similar ZnO-derived bands, while the conduction and valence band edges are slightly shifted due to p–d and s–d interactions. After the Co dopping, the band gap of ZnO becomes narrower, which testifies the better effectiveness related to the light absorption and charge transfer/separation kinetics.

Based on the above data analysis, a reasonable mechanism can be suggested to explain the photocatalytic CO_2 reduction process of ZnO-5%Co-cit. (Fig. 3i) When visible light irradiates on the system, many electron–hole pairs are generated. The electrons on the VB orbitals of ZnO are excited to CB. Due to the

Co doping, the excited electrons can effectively transfer from the CB of ZnO to a doping energy level of ZnO-5%Co-cit. After obtaining photogenerated electrons, ZnO-5%Co-cit utilizes these electrons for photocatalytic reduction of CO_2 to CO and CH_4. In this process, the doped cobalt ions play a crucial role in optimizing the band structure, efficiently transferring and utilizing these photogenerated electrons, which promotes the progress of CO_2 reduction reactions. At the same time, the photogenerated holes on the VB of ZnO-5%Co-cit undergo oxidation reaction with the hole sacrificial agent TEOA. This step not only effectively consumes the photogenerated holes, preventing electron–hole recombination, but also ensures the sustainability of the photocatalytic cycle through the oxidation reaction of TEOA.

Conclusions

In conclusion, cobalt-doped zinc oxide nanoparticles (Co-ZnO NPs) effectively address the challenges of imbalanced charge transfer and utilization in photocatalytic CO_2 reduction. Cobalt doping not only enhances light absorption but also significantly improves charge transfer and separation kinetics, thereby modulating the reduction reaction dynamics. Photocatalytic tests reveal that Co-ZnO NPs achieve a CO yield of 143.90 μmol g^{-1} h^{-1}, which is 15.73 times higher than that of undoped ZnO, and maintains excellent stability. This work provides a new approach to enhancing the efficiency of photoredox catalysis, emphasizing the importance of doping-induced polarization states in optimizing catalytic performance.

Data availability

All data included in this study are available upon request by contact with the corresponding author.

Conflicts of interest

There are no conflicts to declare.

Acknowledgements

We acknowledge to The National Natural Science Foundation of China (NSFC 21801226) and the Natural Science Foundation of Zhejiang Province (LY20B010002 and LY21C120001) and thanks to the Institute of Crystallography and Structural Physics at Friedrich-Alexander-University Erlangen and FATA University/ HEC Pakistan for providing access to various instruments and financial support.

References

1 G. Bonan and S. Doney, Climate, ecosystems, and planetary futures: The challenge to predict life in Earth system models, *Science*, 2018, **359**, eaam8328.
2 H. Chen, *et al.*, The impacts of climate change and human activities on biogeochemical cycles on the Qinghai-Tibetan Plateau, *Global Change Biol.*, 2013, **19**(10), 2940–2955.
3 A. D. Nugroho, I. Y. Prasada and Z. Lakner, Comparing the effect of climate change on agricultural competitiveness in developing and developed countries, *J. Cleaner Prod.*, 2023, **406**, 137139.
4 R. Lindsey and L. Dahlman, *Climate change: Global temperature*, Climate.gov, 2020, vol. 16.
5 P. D. Jones, *et al.*, Surface air temperature and its changes over the past 150 years, *Rev. Geophys.*, 1999, **37**(2), 173–199.
6 R. Ruela, *et al.*, Global and regional evolution of sea surface temperature under climate change, *Glob. Planet. Change.*, 2020, **190**, 103190.
7 J. Houghton, The science of global warming, *Interdiscip. Sci. Rev.*, 2001, **26**(4), 247–257.
8 D. W. Kweku, *et al.*, Greenhouse effect: greenhouse gases and their impact on global warming, *J. Sci. Res.*, 2018, **17**(6), 1–9.
9 K. O. Yoro and M. O. Daramola, CO_2 emission sources, greenhouse gases, and the global warming effect, in *Advances in Carbon Capture*, Elsevier, 2020, pp. 3–28.
10 N. W. Arnell, *et al.*, Global and regional impacts of climate change at different levels of global temperature increase, *Clim. Change*, 2019, **155**, 377–391.
11 A. R. Moss, J.-P. Jouany, and J. Newbold. Methane production by ruminants: its contribution to global warming. in *Annales de zootechnie*, EDP Sciences, 2000.
12 R. de_Richter and S. Caillol, Fighting global warming: The potential of photocatalysis against CO_2, CH_4, N_2O, CFCs, tropospheric O_3, BC and other major contributors to climate change, *J. Photochem. Photobiol. C: Photochem. Rev.*, 2011, **12**(1), 1–19.
13 P. Purohit and L. Höglund-Isaksson, Global emissions of fluorinated greenhouse gases 2005–2050 with abatement potentials and costs, *Atmos. Chem. Phys.*, 2017, **17**(4), 2795–2816.
14 V. L. St. Louis, *et al.*, Reservoir Surfaces as Sources of Greenhouse Gases to the Atmosphere: A Global Estimate: Reservoirs are sources of greenhouse gases to the atmosphere, and their surface areas have increased to the point where they should be included in global inventories of anthropogenic emissions of greenhouse gases, *BioScience*, 2000, **50**(9), 766–775.
15 S. Tahir, M. Rafique and A. Alaamer, Biomass fuel burning and its implications: Deforestation and greenhouse gases emissions in Pakistan, *Environ. Pollut.*, 2010, **158**(7), 2490–2495.
16 R. A. Houghton, Tropical deforestation as a source of greenhouse gas emissions, *Tropical deforestation and climate change*, 2005, vol. 13.
17 Y. Xi-Liu and G. Qing-Xian, Contributions of natural systems and human activity to greenhouse gas emissions, *Adv. Clim. Change Res.*, 2018, **9**(4), 243–252.
18 J. G. Olivier, K. Schure, and J. Peters, *Trends in Global CO_2 and Total Greenhouse Gas Emissions*, PBL Netherlands Environmental Assessment Agency, 2017, vol. 5, pp. 1–11.
19 D. Ehhalt, *et al.*, Atmospheric chemistry and greenhouse gases, *Climate Change 2001: the Scientific Basis*, Intergovernmental panel on climate change, 2001.

20 S. Solomon, *et al.*, Persistence of climate changes due to a range of greenhouse gases, *Proc. Natl. Acad. Sci. U. S. A.*, 2010, **107**(43), 18354–18359.
21 R. Martos-Villa, *et al.*, Crystal structure, stability and spectroscopic properties of methane and CO_2 hydrates, *J. Mol. Graphics Modell.*, 2013, **44**, 253–265.
22 X. Du, *et al.*, CO_2 and CH_4 adsorption on different rank coals: A thermodynamics study of surface potential, Gibbs free energy change and entropy loss, *Fuel*, 2021, **283**, 118886.
23 G. Sahara and O. Ishitani, Efficient photocatalysts for CO_2 reduction, *Inorg. Chem.*, 2015, **54**(11), 5096–5104.
24 M. Dunwell, *et al.*, Understanding Surface-Mediated Electrochemical Reactions: CO_2 Reduction and Beyond, *ACS Catal.*, 2018, **8**(9), 8121–8129.
25 Z. Xiao, *et al.*, A comprehensive review on photo-thermal co-catalytic reduction of CO_2 to value-added chemicals, *Fuel*, 2024, **362**, 130906.
26 H. S. Shafaat and J. Y. Yang, Uniting biological and chemical strategies for selective CO_2 reduction, *Nat. Catal.*, 2021, **4**(11), 928–933.
27 T. Janes, Y. Yang and D. Song, Chemical reduction of CO_2 facilitated by C-nucleophiles, *Chem. Commun.*, 2017, **53**(83), 11390–11398.
28 S. Saeidi, N. A. S. Amin and M. R. Rahimpour, Hydrogenation of CO_2 to value-added products—A review and potential future developments, *J. CO_2 Util.*, 2014, **5**, 66–81.
29 A. Alissandratos and C. J. Easton, Biocatalysis for the application of CO_2 as a chemical feedstock, *Beilstein J. Org. Chem.*, 2015, **11**(1), 2370–2387.
30 B. Weng, *et al.*, Photo-assisted technologies for environmental remediation, *Nat. Rev. Clean Technol.*, 2025, **1**(3), 201–215.
31 H. Huang, *et al.*, Site-Sensitive Selective CO_2 Photoreduction to CO over Gold Nanoparticles, *Angew. Chem., Int. Ed.*, 2022, **61**(28), e202204563.
32 H. Huang, *et al.*, Noble-Metal-Free High-Entropy Alloy Nanoparticles for Efficient Solar-Driven Photocatalytic CO_2 Reduction, *Adv. Mater.*, 2024, **36**(26), e2313209.
33 L. Balode, *et al.*, Pros and Cons of Strategies to Reduce Greenhouse Gas Emissions from Peatlands: Review of Possibilities, *Appl. Sci.*, 2024, **14**(6), 2260.
34 S. Nahar, *et al.*, Advances in photocatalytic CO_2 reduction with water: a review, *Materials*, 2017, **10**(6), 629.
35 H. Zhang, *et al.*, Crystal facet-dependent electrocatalytic performance of metallic Cu in CO_2 reduction reactions, *Chin. Chem. Lett.*, 2022, **33**(8), 3641–3649.
36 S. Fang, *et al.*, Photocatalytic CO_2 reduction, *Nat. Rev. Methods Primers*, 2023, **3**(1), 61.
37 R. Busquets and L. Mbundi, Concepts of nanotechnology, in *Emerging Nanotechnologies in Food Science*, Elsevier, 2017, pp. 1–9.
38 C. N. R. Rao, A. Müller, and A. K. Cheetham, *The Chemistry of Nanomaterials: Synthesis, Properties and Applications*, John Wiley & Sons, 2006.
39 A. B. Asha and R. Narain, Nanomaterials properties, in *Polymer Science and Nanotechnology*, Elsevier, 2020, pp. 343–359.
40 H. Cerjak, *Nanomaterials: an Introduction to Synthesis, Properties and Applications*, Taylor & Francis, 2009.
41 S. P. Douglas, S. Mrig and C. E. Knapp, MODs vs. NPs: Vying for the future of printed electronics, *Chem.–Eur. J.*, 2021, **27**(31), 8062–8081.
42 B. A. Yousef, K. Elsaid and M. A. Abdelkareem, Potential of nanoparticles in solar thermal energy storage, *Therm. Sci. Eng. Prog.*, 2021, **25**, 101003.
43 M. Fathi-Achachelouei, *et al.*, Use of nanoparticles in tissue engineering and regenerative medicine, *Front. Bioeng. Biotechnol.*, 2019, **7**, 113.
44 M. L. Carrillo-Inungaray, *et al.*, Use of nanoparticles in the food industry: advances and perspectives, *Impact of Nanoscience in the Food Industry*, 2018, pp. 419–444.
45 M. Thiruvengadam, G. Rajakumar and I.-M. Chung, Nanotechnology: current uses and future applications in the food industry, *3 Biotech*, 2018, **8**, 1–13.
46 X. Qiu, *et al.*, Applications of Nanomaterials in Asymmetric Photocatalysis: Recent Progress, Challenges, and Opportunities, *Adv. Mater.*, 2021, **33**(6), 2001731.
47 A. Fujishima and X. Zhang, Titanium dioxide photocatalysis: present situation and future approaches, *C. R. Chim.*, 2006, **9**(5–6), 750–760.
48 C. B. Ong, L. Y. Ng and A. W. Mohammad, A review of ZnO nanoparticles as solar photocatalysts: Synthesis, mechanisms and applications, *Renewable Sustainable Energy Rev.*, 2018, **81**, 536–551.
49 W. Hussain, *et al.*, Synthesis and characterization of CdS photocatalyst with different morphologies: visible light activated dyes degradation study, *Kinet. Catal.*, 2018, **59**, 710–719.
50 S. Guo, *et al.*, Au NPs@ MoS_2 sub-micrometer sphere-ZnO nanorod hybrid structures for efficient photocatalytic hydrogen evolution with excellent stability, *Small*, 2016, **12**(41), 5692–5701.
51 Z. Zheng, *et al.*, Plasmon-enhanced solar water splitting on metal-semiconductor photocatalysts, *Chem.–Eur. J.*, 2018, **24**(69), 18322–18333.
52 A. Naveed Ul Haq, *et al.*, Synthesis approaches of zinc oxide nanoparticles: the dilemma of ecotoxicity, *J. Nanomater.*, 2017, **2017**(1), 8510342.
53 W. K. Choi, *et al.*, A combined top-down and bottom-up approach for precise placement of metal nanoparticles on silicon, *Small*, 2008, **4**(3), 330–333.
54 A. Gour and N. K. Jain, Advances in green synthesis of nanoparticles, *Artif. Cells, Nanomed., Biotechnol.*, 2019, **47**(1), 844–851.
55 V. Arole and S. Munde, Fabrication of nanomaterials by top-down and bottom-up approaches-an overview, *J. Mater. Sci.*, 2014, **1**, 89–93.
56 S. Mourdikoudis, R. M. Pallares and N. T. Thanh, Characterization techniques for nanoparticles: comparison and complementarity upon studying nanoparticle properties, *Nanoscale*, 2018, **10**(27), 12871–12934.

57 K. Simeonidis, *et al.*, Inorganic engineered nanoparticles in drinking water treatment: a critical review, *Environ. Sci.:Water Res. Technol.*, 2016, **2**(1), 43–70.
58 P. Biswas and C.-Y. Wu, Nanoparticles and the environment, *J. Air Waste Manage. Assoc.*, 2005, **55**(6), 708–746.
59 S. K. Patel, J.-K. Lee and V. C. Kalia, Nanoparticles in biological hydrogen production: an overview, *Indian J. Microbiol.*, 2018, **58**, 8–18.
60 Y. Chen, C. W. Li and M. W. Kanan, Aqueous CO_2 reduction at very low overpotential on oxide-derived Au nanoparticles, *J. Am. Chem. Soc.*, 2012, **134**(49), 19969–19972.
61 O. Ola and M. M. Maroto-Valer, Transition metal oxide based TiO_2 nanoparticles for visible light induced CO_2 photoreduction, *Appl. Catal., A*, 2015, **502**, 114–121.
62 J. Ran, M. Jaroniec and S. Z. Qiao, Cocatalysts in semiconductor-based photocatalytic CO_2 reduction: achievements, challenges, and opportunities, *Adv. Mater.*, 2018, **30**(7), 1704649.
63 J. Low, B. Cheng and J. Yu, Surface modification and enhanced photocatalytic CO_2 reduction performance of TiO_2: a review, *Appl. Surf. Sci.*, 2017, **392**, 658–686.
64 I. I. Alkhatib, *et al.*, Metal-organic frameworks for photocatalytic CO_2 reduction under visible radiation: A review of strategies and applications, *Catal. Today*, 2020, **340**, 209–224.
65 Z. Tang, *et al.*, Facet selectivity of ligands on silver nanoplates: Molecular mechanics study, *J. Phys. Chem. C*, 2014, **118**(37), 21589–21598.
66 F. Liu, *et al.*, Transfer Channel of Photoinduced Holes on a TiO_2 Surface As Revealed by Solid-State Nuclear Magnetic Resonance and Electron Spin Resonance Spectroscopy, *J. Am. Chem. Soc.*, 2017, **139**, 10020.
67 H. Dong, *et al.*, Dual Metallosalen-Based Covalent Organic Frameworks for Artificial Photosynthetic Diluted CO_2 Reduction, *Angew. Chem., Int. Ed.*, 2025, **64**(2), e202414287.
68 H. Dong, *et al.*, Regulation of metal ions in smart metal-cluster nodes of metal-organic frameworks with open metal sites for improved photocatalytic CO_2 reduction reaction, *Appl. Catal., B*, 2020, **276**, 119173.
69 H. Dong, *et al.*, Covalently anchoring covalent organic framework on carbon nanotubes for highly efficient electrocatalytic CO_2 reduction, *Appl. Catal., B*, 2022, **303**, 120897.
70 L. Spanhel and M. A. Anderson, Semiconductor clusters in the sol-gel process: quantized aggregation, gelation, and crystal growth in concentrated zinc oxide colloids, *J. Am. Chem. Soc.*, 1991, **113**(8), 2826–2833.
71 A. Wood, *et al.*, Size effects in ZnO: the cluster to quantum dot transition, *Aust. J. Chem.*, 2003, **56**(10), 1051–1057.
72 C. Chory, *et al.*, Influence of liquid-phase synthesis parameters on particle sizes and structural properties of nanocrystalline ZnO powders, *Phys. Status Solidi C*, 2007, **4**(9), 3260–3269.
73 I. Ullah, *et al.*, Antimicrobial activities and neuroprotective potential for Alzheimer's disease of pure, Mn, Co, and Al-doped ZnO ultra-small nanoparticles, *Green Process. Synth.*, 2024, **13**(1), 20240096.
74 H. Wang, *et al.*, Tailoring CO_2 Adsorption Configuration with Spatial Confinement Switches Electroreduction Product from Formate to Acetate, *J. Am. Chem. Soc.*, 2025, **147**(7), 6095–6107.
75 H. Huang, *et al.*, Noble-Metal-Free High-Entropy Alloy Nanoparticles for Efficient Solar-Driven Photocatalytic CO_2 Reduction, *Adv. Mater.*, 2024, **36**(26), 2313209.